Time-Domain Aeroservoelastic Modeling Using Weighted Unsteady Aerodynamic Forces

Mordechay Karpel*
Technion—Israel Institute of Technology, Haifa, Israel

A modeling method for constructing a state-space aeroservoelastic mathematical model for time-domain analysis with a low number of aerodynamic lag states is presented. The modeling method employs the minimum-state method for rational approximation of tabulated unsteady aerodynamic force coefficients at various reduced-frequency values. The approximation method is modified to deal with weighted aerodynamic data and with alternative constraint combinations. Two weighting types are analyzed and discussed. The first weighting is normalizing the aerodynamic data to maximum unit value of each aerodynamic coefficient. The second weighting is one in which each tabulated coefficient, at each reduced-frequency value, is weighted according to the effect of an incremental error of this coefficient on aeroelastic characteristics of the system. This weighting yields a better fit of the more important terms at the expense of less important ones. The analytical developments are presented and numerical examples, which demonstrate various features of this method, are shown to yield significant reduction in model size per given accuracy relative to other rational approximation methods.

Introduction

AEROSERVOELASTICITY deals with interaction between aeroelastic and control system characteristics of a flight vehicle. The motion of the control surfaces excites the aeroelastic system and causes structural vibrations. The vibrations are sensed by the control sensors and fed back, through the control transfer function, to the control surface actuators. This closes the aeroservoelastic loop and affects the airframe stability characteristics.

Various control analyses, design, and simulation techniques require the equations of motion to be cast in a linear time-invariant state-space form. In order to account for unsteady aerodynamics, the aerodynamic forces have to be described as a rational function of the Laplace variable s, as has been shown in various applications such as those of Sevart,[1] Edwards,[2] Roger,[3] and Vepa.[4] The resulting state-space equations include augmented states that represent the aerodynamic lags. The number of the augmented states is a function of the number of denominator roots in the rational approximation.

Systematic techniques that use oscillatory aerodynamic matrices (defined along the imaginary axis of the s plane) to generate rational approximate solutions for arbitrary motion were developed by several authors. Roger et al.[5] introduced the Pade approximate technique in which each term of the aerodynamic matrix is approximated by a different ratio of polynomials in s. In this technique, there is one additional augmented state per each root of each term in the aerodynamic matrix. Roger[3] realized that the aerodynamic matrix can be approximated more efficiently by using common denominator roots. He used a least-square technique for a term-by-term fitting of the tabulated aerodynamic matrices. Vepa[4] introduced a matrix Pade approximate technique that approximates the entire aerodynamic matrix by a ratio of matrix polynomials. Various modifications of the matrix Pade technique were suggested by Edwards,[2] Karpel,[6] and Dunn.[7] For the case of irreversible controls, the number of aerodynamic augmented states resulting from these methods is equal to the number of denominator roots, multiplied by either the number of vibration modes (in Roger's method) or the sum of vibration, control, and gust modes (in the matrix Pade methods).

Karpel[6,8] introduced the minimum-state approximation method in which a higher number of denominator roots is required per given accuracy. However, the number of augmented states resulting from this method is equal to the number of the denominator roots, regardless of the number of modes. Application to an aeroelastic model with three vibration modes and one control mode showed that the minimum-state method yields less than half the number of augmented states resulting from the previous methods with the same level of accuracy. The minimum-state approximation solution of Refs. 6 and 8 implies perfect fit of the steady aerodynamics and of the aerodynamic matrix at one other reduced-frequency value to be chosen by the analyst. A nonlinear iterative least-square technique is used to approximate the other tabulated aerodynamic matrices.

Tiffany and Adams[9-11] extended Roger's method, the modified matrix Pade method, and the minimum-state method to include the capability for enforcing or relaxing various equality constraints as desired by the analyst. These extensions, abbreviated by ELS, EMMP, and EMS, respectively, are the optional approximation methods in the Interaction of Structures, Aerodynamics, and Controls (ISAC) computer program, a recent version of Ref. 15. One effect of this extension on the minimum-state method was a very large increase in the number of equations solved simultaneously in every least-square iteration step. Consequently, the iterative process was severely slowed, and computational considerations limited the problem size. A comparative study[11] with a seven-mode aeroelastic model shows that the minimum-state method can cut the number of augmented states per desired accuracy by a factor of 2 or more. Nonlinear programming techniques were used in these applications to optimize the values of the approximation roots with respect to an overall error function. Their experience was that the application of this optimization to the minimum-state method is more tedious than to the other methods.

Received March 14, 1988; revision received Aug. 9, 1988.

*Senior Research Associate, Department of Aerospace Engineering; currently NRC Research Associate, NASA Langley Research Center, Hampton, VA.

On the other hand, since the minimum-state method allows more distinct approximation roots and yields less augmented states than in other methods, optimization of the root values is not as important.

Until now, most approximation methods treated the different tabulated aerodynamic terms as equally important (except for the imposed equality constraint points). Dunn[7] allowed a frequency-dependent data weighting matrix to be defined by the user. One of the main purposes of this work is to develop a weighting algorithm that weights different data terms according to the effect of their errors on aeroelastic characteristics. Other purposes are to formulate the aeroservoelastic model using the minimum-state approximation, to modify the original minimum-state formulation to accept weighted data, to allow more constraint options without increasing the problem size, and to investigate the various aspects of the modified method with numerical examples of larger size than before.

Aeroservoelastic Formulation

The common approach for formulating the equations of motion of an aeroelastic system[12] starts with normal modes analysis of the structural system. A set of low-frequency vibration modes (that may include rigid-body modes) is chosen to represent the structural motion in generalized coordinates. Aeroservoelastic formulation requires additional modes that represent the control surface commanded deflections. These are defined here by a 1-rad rotation of a control surface and zero deflections elsewhere. Gust velocity modes may also be required.

A generalized unsteady aerodynamic complex force coefficient matrix $[Q]$ is defined by the Laplace transform of its partitions as

$$\begin{Bmatrix} F_s(s) \\ F_c(s) \end{Bmatrix} = q \begin{bmatrix} Q_{ss}(s) & Q_{sc}(s) \\ Q_{cs}(s) & Q_{cc}(s) \end{bmatrix} \begin{Bmatrix} \xi(s) \\ \delta_c(s) \end{Bmatrix} + \frac{q}{V} \begin{bmatrix} Q_{sg}(s) \\ Q_{cg}(s) \end{bmatrix} \{w(s)\} \tag{1}$$

where $\{F_s\}$ is the vector of generalized aerodynamic forces on the vibration modes, $\{F_c\}$ the vector of control surface aerodynamic hinge moments, $\{\xi\}$ the vector of generalized structural displacements, $\{w\}$ the gust velocity vector, and $\{\delta_c\}$ the vector of control surface commanded deflections, namely, the actuator outputs (in radians).

For the sake of simplicity, the gust terms are omitted for the formulation in the rest of this section. The Laplace transform of the open-loop aeroelastic system equation of motion, excited by control surface motion, are

$$[C(s)]\{\xi(s)\} = (q[Q_{sc}(s)] - s^2[M_{sc}])\{\delta_c(s)\} \tag{2a}$$

where

$$[C(s)] = [M_s]s^2 + [B_s]s + [K_s] - q[Q_{ss}(s)] \tag{2b}$$

where $[M_s]$, $[B_s]$, and $[K_s]$ are the generalized structural mass, damping, and stiffness matrices, respectively, and $[M_{sc}]$ is the coupling mass matrix between the control and the structural modes. The total hinge moment vector (aerodynamic and inertial) is

$$\{T_c(s)\} = (q[Q_{cs}(s)] - s^2[M_{sc}]^T)\{\xi(s)\} + (q[Q_{cc}(s)] - s^2[M_{cc}])\{\delta_c(s)\} \tag{3}$$

where $[M_{cc}]$ is a diagonal matrix of control surface moments of inertia about the hinge line.

In order to transform Eqs. (2) and (3) into time-domain constant coefficient equations, the aerodynamic matrices have to be described as rational functions of s. The minimum-state method[6] approximates $[Q(s)]$ by

$$[\tilde{Q}(\bar{s})] = [A_0] + [A_1]\bar{s} + [A_2]\bar{s}^2 + [D](\bar{s}[I] - [R])^{-1}[E]\bar{s} \tag{4}$$

where $\bar{s}$ is the nondimensionalized Laplace variable:

$$\bar{s} = s\,b/V \tag{5}$$

The real-valued approximation matrices of Eq. (4) are partitioned as

$$[A_i] = \begin{bmatrix} A_{ss_i} & A_{sc_i} \\ A_{cs_i} & A_{cc_i} \end{bmatrix}, \quad [D] = \begin{bmatrix} D_s \\ D_c \end{bmatrix}, \quad [E] = [E_s E_c] \tag{6}$$

An augmented state vector is now defined by its Laplace transform as

$$\{x_a(s)\} = (\bar{s}[I] - [R])^{-1}([E_s]\{\xi(s)\} + [E_c]\{\delta_c(s)\})\bar{s} \tag{7}$$

or, with the substitution of Eq. (5),

$$s\{x_a(s)\} = s[E_s]\{\xi(s)\} + s[E_c]\{\delta_c(s)\} + \frac{V}{b}[R]\{x_a(s)\} \tag{8}$$

The substitution of Eq. (4) into Eq. (2), while using the partitions of Eq. (6), and Eq. (5) and (7), yields

$$([\bar{M}_s]s^2 + [\bar{B}_s]s + [\bar{K}_s])\{\xi(s)\} - q[D_s]\{x_a(s)\} = (-[\bar{M}_{sc}]s^2 + [\bar{B}_{sc}]s + [\bar{K}_{sc}])\{\delta_c(s)\} \tag{9}$$

where

$$[\bar{M}_s] = [M_s] - \frac{\rho b^2}{2}[A_{ss_2}], \qquad [\bar{B}_s] = [B_s] - \frac{\rho b V}{2}[A_{ss_1}]$$

$$[\bar{K}_s] = [K_s] - q[A_{ss_0}], \qquad [\bar{M}_{sc}] = [M_{sc}] - \frac{\rho b^2}{2}[A_{sc_2}]$$

$$[\bar{B}_{sc}] = \frac{\rho b V}{2}[A_{sc_1}], \qquad [\bar{K}_{sc}] = q[A_{sc_0}] \tag{10}$$

The time-domain state-space open-loop equation resulting from Eqs. (8) and (9) is

$$\{\dot{x}\} = [A]\{x\} + [B]\{u\} \tag{11}$$

where

$$\{x\} = \begin{Bmatrix} \xi \\ \dot{\xi} \\ x_a \end{Bmatrix}, \qquad [A] = \begin{bmatrix} 0 & I & 0 \\ -\bar{M}_s^{-1}\bar{K}_s & -\bar{M}_s^{-1}\bar{B}_s & q\bar{M}_s^{-1}D_s \\ 0 & E_s & \frac{V}{b}R \end{bmatrix}$$

$$[B] = \begin{bmatrix} 0 & 0 & 0 \\ \bar{M}_s^{-1}\bar{K}_{sc} & \bar{M}_s^{-1}\bar{B}_{sc} & -\bar{M}_s^{-1}M_{sc} \\ 0 & E_c & 0 \end{bmatrix}, \quad \{u\} = \begin{Bmatrix} \delta \\ \dot{\delta} \\ \ddot{\delta} \end{Bmatrix} \tag{12}$$

The substitution of the hinge moment related partitions of Eq. (4) into Eq. (3), while using Eqs. (5) and (7), yields

$$\{T_c(s)\} = (-[\bar{M}_{cs}]s^2 + [\bar{B}_{cs}]s + [\bar{K}_{cs}])\{\xi(s)\} + (-[\bar{M}_{cc}]s^2 + [\bar{B}_{cc}]s + [\bar{K}_{cc}])\{\delta_c(s)\} + q[D_c]\{x_a(s)\} \tag{13}$$

where

$$[\bar{M}_{cs}] = [M_{cs}]^T - \frac{\rho b^2}{2}[A_{cs_2}], \qquad [\bar{B}_{cs}] = \frac{\rho b V}{2}[A_{cs_1}]$$

$$[\bar{K}_{cs}] = q[A_{cs_0}], \qquad [\bar{M}_{cc}] = [M_{cc}] - \frac{\rho b^2}{2}[A_{cc_2}]$$

$$[\bar{B}_{cc}] = \frac{\rho b V}{2}[A_{cc_1}], \qquad [\bar{K}_{cc}] = q[A_{cc_0}]$$

The hinge moments time history can now be related to the state and control vectors of Eq. (11) by

$$\{T_c\} = [H_c]\{x\} + [J_c]\{u\} \tag{14}$$

where

$$[H_c] = [\bar{K}_{cs}\bar{B}_{cs}\ qD_c] + \bar{M}_{cs}\bar{M}_s^{-1}[\bar{K}s\ \bar{B}_s\ -qD_s]$$

$$[J_c] = [\bar{K}_{cc}\bar{B}_c\ -\bar{M}_c] - \bar{M}_{cs}\bar{M}_s^{-1}[\bar{K}_{sc}\bar{B}_{sc}\ -\bar{M}_{sc}]$$

Structural displacement measurements are related to the generalized displacements by

$$\{y\} = [\Psi_m]\{\xi\} \tag{15}$$

where $[\Psi_m]$ is the matrix of modal deflections at the sensor input points. For structural velocity or acceleration measurements, $\{\xi\}$ of Eq. (15) is replaced by $\{\dot{\xi}\}$ or $\{\ddot{\xi}\}$. The hinge moments may also be considered as a part of the output vector $\{y\}$. All of these measurements can be cast in the state-space control formulation [using Eqs. (11), (12), (14), and (15)] as

$$\{y\} = [H]\{x\} + [J]\{u\} \tag{16}$$

A gust vector consisting of $\{w\}$ and $\{\dot{w}\}$ can be added to the right-hand side of Eqs. (11), (14), and (16) for gust response analysis. The formulation follows that of the control surface related columns, with the exceptions that there are no mass-related terms and that the $[A_{sg_2}]$ and $[A_{cg_2}]$ portions of $[A_2]$ in Eq. (4) are constrained to be zero. This suppresses all $\{\ddot{w}\}$-related terms.

Until now we dealt with the structural and aerodynamic portions of the aeroservoelastic model. The control loop is closed by connecting the control column $\{u\}$ to the measurement vector $\{y\}$ through the control system transfer functions. The Laplace transform of this connection may be formulated as

$$\{\delta(s)\} = [T(s)][\Psi_m]\ \{\xi(s)\} + [T_h(s)]\ \{T_c(s)\} \tag{17}$$

where $[T(s)]$ is a matrix of transfer functions that includes the effects of measurement type, sensor dynamics, control laws, and actuator dynamics. $[T_h(s)]$ is a diagonal matrix of transfer functions that reflects the effect of hinge moments on the actuator dynamics. This term is neglected when the actuators are assumed to be irreversible.

To complete the state-space formulation, the state vector of Eq. (11) is augmented by control system states, and the system matrices in Eqs. (12) and (16) are modified according to the specific nature of the transfer functions of Eq. (17). This (problem-related) part of the aeroservoelastic modeling is beyond the scope of this paper. Various examples of time-domain modeling, analysis, design, and simulation of the control system part of the aeroservoelastic problem are given in Refs. 2, 5, 6, 8, and 13–15.

Minimum-State Approximation Procedure

The full development of the minimum-state method is given in Refs. 6 and 8. Key equations are repeated here, the least-square solution is modified to deal with weighted data, and alternative constraints are added. The input data are unsteady aerodynamic complex matrices calculated for several reduced-frequency values ($k = \omega b/V$) along the imaginary axis of the Laplace plane, namely, at various $\bar{s} = ik$ points. The aerodynamic approximation of Eq. (4) for imaginary values of $\bar{s}$ is

$$[\bar{Q}(ik)] = [A_0] + [A_1]ik - [A_2]k^2 + [D](ik[I] - [R])^{-1}[E]ik \tag{18}$$

Separation of Eq. (18) into real and imaginary parts gives

$$[\bar{F}(k)] = [A_0] - [A_2]k^2 + k^2[D](k^2[I] + [R]^2)^{-1}[E] \tag{19}$$

and

$$[\bar{G}(k)] = [A_1]k - k[D](k^2[I] + [R]^2)^{-1}[R][E] \tag{20}$$

Three constraints are applied to each term of $[\bar{Q}(ik)]$ in order to eliminate $[A_0]$, $[A_1]$, and $[A_2]$ from the approximation equations. The formulation that follows is for the case of data match constraints where all the terms of $[\bar{Q}(ik)]$ are assigned with the same set of constraints. Alternative constraints are discussed at the end of this section. The three constraints are matching the real part of the tabulated data at $k = 0$ and at $k_f \neq 0$, and matching the imaginary part of the tabulated data at $k_g \neq 0$, which yields

$$[A_0] = [F(0)] \tag{21}$$

$$[A_1] = [G(k_g)]/k_g + [D](k_g^2[I] + [R]^2)^{-1}[R][E] \tag{22}$$

$$[A_2] = ([F(0)] - [F(k_f)])/k_f^2 + [D](k_f^2[I] + [R]^2)^{-1}[E] \tag{23}$$

At other tabulated k_ℓ values

$$k_\ell^2\ [D][\bar{C}_f(k_\ell)][E] \approx [\bar{F}(k_i)] \tag{24a}$$

and

$$k_\ell[D][\bar{C}_g(k_\ell)][R][E] \approx [\bar{G}(k_i)] \tag{24b}$$

where

$$[\bar{C}_f(k)] = (k^2[I] + [R]^2)^{-1} - (k_f^2[I] + [R]^2)^{-1} \tag{25a}$$

$$[\bar{C}_g(k)] = (k^2[I] + [R]^2)^{-1} - (k_g^2[I] + [R]^2)^{-1} \tag{25b}$$

$$[\bar{F}(k)] = ([F(k)] - [F(0)]) - ([F(k_f)] - [F(0)])(k^2/k_f^2) \tag{25c}$$

$$[\bar{G}(k)] = [G(k_f)](k/k_f) - [G(k)] \tag{25d}$$

$[R]$ is a diagonal matrix with distinct negative terms. For a given $[R]$ and an initial value of $[D]$, and where Eqs. (24) provide an approximation to be solved by the weighted least-square method[16] for each column of $[E]$. The least-square equation for the ith column of $[E]$ is

$$\left(\sum_\ell [A_\ell]^T[W_{j\ell}^2][A_\ell]\right)\{E_j\} = \sum_\ell [A_\ell]^T[W_{j\ell}^2]\{b_\ell\} \tag{26}$$

where

$$[A_\ell] = \begin{bmatrix} k_\ell^2 D\bar{C}_f(k_\ell) \\ k_\ell D\bar{C}_g(k_\ell)R \end{bmatrix}, \qquad \{b_\ell\} = \begin{Bmatrix} \bar{F}_j(k_\ell) \\ \bar{G}_j(k_\ell) \end{Bmatrix} \tag{27}$$

and the terms of the diagonal matrix $[W_{j\ell}^2]$ are the squared weights assigned to the rows of the jth column of $[Q(ik_\ell)]$; $\{\bar{F}_j(k_\ell)\}$ and $\{\bar{G}_j(k_\ell)\}$ are the jth columns of $[\bar{F}(k_\ell)]$ and $[\bar{G}(k_\ell)]$ of Eqs. (24).

After solving for $[E]$, least-square equations are set and solved for the rows of $[D]$:

$$\left(\sum_\ell [A_\ell^*]^T[W_{i\ell}^2][A_\ell^*]\right)\{D_i^T\} = \sum_\ell [A_\ell^*]^T[W_{j\ell}^2]\{b_\ell^*\} \tag{28}$$

where

$$[A_\ell^*] = \begin{bmatrix} k_\ell^2 E^T\bar{C}_f(k_\ell) \\ k_\ell E^T R\bar{C}_g(k_\ell) \end{bmatrix}, \qquad \{b_\ell^*\} = \begin{Bmatrix} \bar{F}_i(k_\ell) \\ \bar{G}_i(k_\ell) \end{Bmatrix} \tag{29}$$

and the terms of the diagonal matrix $[W_{i\ell}^2]$ are the squared weights assigned to the columns of the ith row of $[Q(ik_\ell)]$; $\{\bar{F}_i(k_\ell)\}^T$ and $\{[\bar{G}_i(k_\ell)\}^T$ are the ith rows of $[\bar{F}(k_\ell)]$ and $[\bar{G}(k_\ell)]$. The procedure repeats alternate solutions for $[E]$ and $[D]$ until convergence is obtained. The initial values of the $n \times m$ $[D]$ matrix, where m is the number of approximation roots and n the number of modes, are up to the choice of the analyst. The default choice is a zero matrix except for all D_{ii} and $D_{(n+i)i}$ (when $n > m$) or D_i $(m+i)$ (when $m > n$), which are equal to 1. After each $[D] \rightarrow [E] \rightarrow [D]$ cycle, the procedure calculates the overall error:

$$\epsilon_t = \sqrt{\sum_{i,j,\ell} \epsilon_{ij\ell}^2} \tag{30}$$

where

$$\epsilon_{ij\ell} = |\tilde{Q}_{ij}(ik_\ell) - Q_{ij}(ik_\ell)|\, W_{ij\ell}$$

Even though the preceding formulation assumed that the same data match constraints are assigned to all the terms of $[\tilde{Q}(ik)]$, one may assign different sets of k_f and k_g values to different (i,j) terms. Each term in Eqs. (22) and (23) and in $[\bar{G}]$ and $[\bar{F}]$ of Eqs. (25) is calculated with its assigned k_f or k_g. The k_f and k_g to be used in $[\bar{C}_f]$ and $[\bar{G}_g]$ of Eqs. (25) are determined when they are applied to Eqs. (27) and (29) according to the associated indices of $\{E_j\}$ and $|D_i|$. An example of using $k_i \neq k_g$ is when one wants to constrain $\partial\tilde{Q}/\partial(ik)$ at $k=0$ to match that of the tabulated data, in order to obtain accurate aerodynamic coefficients associated with rigid-body velocities. This is done by assigning $k_g = k_2$ to the terms associated with the rigid-body modes (assuming that $k_2 \rightarrow 0$). On the other hand, assignment of $k_f = k_2$ when $k_2 \rightarrow 0$ might cause numerical problems.

Another possible constraint is $A_{2_{ij}} = 0$ (no "aerodynamic mass" terms). This constraint replaces the real-part matching condition at $k = k_f$ of Eq. (23). As a result, whenever $|D_i|$ and $\{E_j\}$ are considered, $[\bar{C}_f(ik_\ell)]$ and the (i,j) term of $[\bar{F}(k_\ell)]$ in Eqs. (27) and (29) appear without the second part of their definition in Eqs. (25). This constraint is assigned, for example, to the gust columns of $[\tilde{Q}]$.

Normalizing the Data

The tabulated values of $[Q(ik_\ell)]$ are a function of the way the modes are normalized. If, for example, the ith mode is multiplied by 2, the ith row and the ith column of the aerodynamic matrix of Eq. (1) are also multiplied by 2 [the (i,i) term is multiplied by 4]. Since the same factors are also applied to the structural matrices, this multiplication should have no effect on the system characteristics. However, without weighting, such multiplication would cause the minimum-state least-square solutions to put more emphasis on the ith-mode-related terms at the expense of others. To avoid this mode normalization dependency, weights are defined by

$$W_{ij\ell} = \frac{1}{\max_{\ell}\{|Q_{ij}(ik_\ell)|, 1\}} \tag{31}$$

The absolute value of a weighted aerodynamic term is

$$\tilde{Q}_{ij}(k_\ell) = W_{ij\ell}\,|Q_{ij}(ik_\ell)| \tag{32}$$

All $W_{ij\ell}$ weights for a given (i,j) pair of indices as defined by Eq. (31) are equal. The ℓ index is retained because it is required in the physical weighting of the next section. The effect of Eq. (31) is normalization of the input data such that the maximum $\tilde{Q}(k_\ell)$ of each (i,j) term is 1, with the exception of terms with maximum $|Q(ik_\ell)|$ of less than 1, which are not normalized. With this weighting, ϵ_t of Eq. (30) is consistent with the "common measure of approximation performance" of Ref. 11.

Physical Weighting

The weighting suggested in this section is designed to weight each term of the tabulated data according to a "measure of importance," which is based on the partial derivative of a selected open-loop characteristic parameter at nominal (stable) flow conditions with respect to the weighted term. Four groups of weights are defined. The first three groups are related to $[Q_{ss}]$, $[Q_{sc}]$, and $\{Q_{cg}\}$ of Eq. (1), respectively. The fourth group encompasses $[Q_{cs}]$, $[Q_{cc}]$, and $\{Q_{cg}\}$. The resulting weight matrices $[W]_\ell$ are a function of k_ℓ. The physically weighted aerodynamic terms below are not a function of the way the modes are normalized and have a maximum value of 1 assigned to one term only in each group.

The weighting of $[Q_{ss}]$ is based on the open-loop system determinant in Eq. (2):

$$\|C(ik)\| = \left\| -[M_s]\frac{k^2V^2}{b^2} + i[B_s]\frac{kV}{b} + [K_s] - q[Q_s(ik)] \right\| \tag{33}$$

The derivative of $\|C(ik)\|$ with respect to $Q_{ss_{ij}}$ is

$$\frac{\partial\|C(ik)\|}{\partial Q_{ss_{ij}}} = -qx\ \text{cofactor}(C_{ij}(k)) \tag{34}$$

Based on this derivative, a measure for the importance of $Q_{ss_{ij\ell}}$ is defined as

$$\bar{W}_{ss_{ij\ell}} = \left| \frac{\text{cofactor}(C_{ij}(k))}{\|C(ik_\ell)\|} \right| \tag{35}$$

This definition assigns more importance to k values at which the open-loop system is closer to instability. The right-hand side of Eq. (35) is actually the absolute value of the (j,i) term of $[C(ik)]^{-1}$. The weight matrices associated with the tabulated $[Q_{ss}]$ matrices are now defined as

$$[W_{ss}]_\ell = \frac{|[C(ik_\ell)]^{-1}|^T}{\max_{i,j,\ell}\{|Q_{ss_{ij}}(ik_\ell)|\,\bar{W}_{ss_{ij\ell}}\}} \tag{36}$$

The weighting of $[Q_{sc}]$ is based on the open-loop actuator output response to sinusoidal excitation by the control surfaces. The vibrations mode response to sinusoidal excitation of unit amplitude by the jth control surface is derived from Eq. (2):

$$\{\xi(i\omega)\} = [C(i\omega)]^{-1}(q\{Q_{sc_j}(i\omega)\} + \omega^2\{M_{sc_j}\}) \tag{37}$$

The open-loop frequency response of the jth actuator to excitation by the jth control surface is derived from Eqs. (17) and (37):

$$\delta_{c_j}(i\omega) = |T_j(i\omega)|\,[\Psi_m][C(i\omega)]^{-1}(q\{Q_{sc_j}(i\omega)\} + \omega^2\{M_{sc_j}\}) \tag{38}$$

where $|T_j(i\omega)|$ is derived from the jth row of $[T(s)]$ of Eq. (17). The measure of importance here is the absolute value of the partial derivative of δ_{c_j} with respect to $Q_{sc_{ij}}$, which yields the measure-of-importance matrix

$$[\bar{W}_{sc}]_\ell = q\,|[T(ik_\ell)][\Psi_m][C(ik_\ell)]^{-1}|^T \tag{39}$$

The resulting weight matrices associated with the tabulated $[Q_{sc}]$ matrices are

$$[W_{sc}]_\ell = \frac{[\bar{W}_{sc}]_\ell}{\max_{i,j,\ell}\{|Q_{sc_{ij}}(ik_\ell)|\,\bar{W}_{sc_{ij\ell}}\}} \tag{40}$$

The weighting of $[Q_{sg}]$ is based on the power spectral density (PSD) of the open-loop response of selected structural acceler-

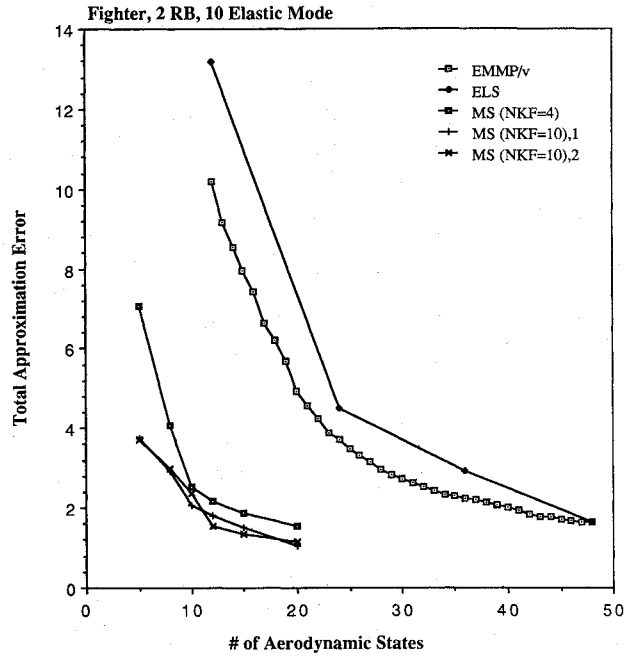

Fig. 1 Total approximation errors of various methods vs number of aerodynamic lag states, 12 vibration modes of a fighter aircraft.

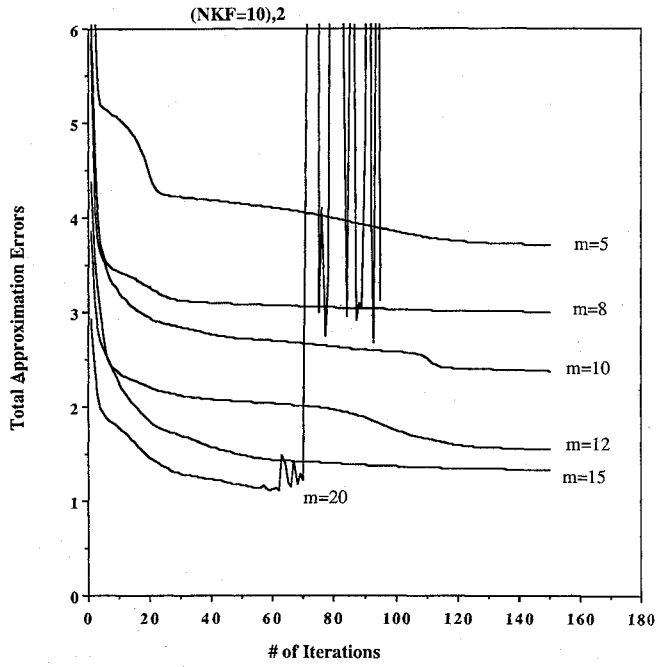

Fig. 2 Minimum-state error convergence vs number of $D \rightarrow E \rightarrow D$ iterations.

ation parameters to continuous gust. The PSD of the response associated with the jth gust is

$$\Phi_{z_j}(\omega) = \left| \frac{\omega^2 q}{V} [\Psi_{z_j}] [C(i\omega)]^{-1} \{Q_{sg_j}(i\omega)\} \right|^2 \Phi_{w_j}(\omega) \tag{41}$$

where $[\Psi_{z_j}]$ is the vector of modal deflections at the jth selected point, and $\Phi_{w_j}(\omega)$ is the Dryden[17] continuous gust PSD. The measure of importance of $Q_{sg_{ij}}$ is the partial derivative of $\sqrt{\Phi_{z_j}(\omega)}$ with respect to $Q_{sg_{ij}}$, which yields

$$[\bar{W}_{sg}]_\ell = \left| \frac{k_\ell^2 q V}{b^2} [\Psi_z] [C(ik_\ell)]^{-1} \right|^T [\sqrt{\Phi_w(k_\ell)}] \tag{42}$$

The resulting weight matrices associated with the tabulated $[Q_{sg}]$ matrices are

$$[W_{sc}]_\ell = \frac{[\bar{W}_{sg}]_\ell}{\max\limits_{i,j,\ell} \{ |Q_{sg_{ij}}(ik_\ell)| \bar{W}_{sg_{ij\ell}} \}} \tag{43}$$

The weighting of the fourth group, the hinge-moment-related terms, is based on hinge-moment response to sinusoidal excitation by the control surfaces. The ith hinge-moment response to excitation by the ith control surface is derived from Eqs. (3) and (2):

$$T_{c_{ii}}(i\omega) = (q\, [Q_{sc_i}(i\omega)] + \omega^2 \{M_{sc_i}\}^T)[C(i\omega)]^{-1}(q\, \{Q_{sc_i}(i\omega)\} + \omega^2 \{M_{sc_i}\}) + q Q_{cc_{ii}}(i\omega) + \omega^2 M_{cc_{ii}} \tag{44}$$

The derivative of Eq. (44) with respect to $Q_{cs_{ij}}$ is

$$\frac{\partial T_{c_{ii}}(i\omega)}{\partial Q_{cs_{ij}}} = q\, [\hat{C}_i(i\omega)] (q\, \{Q_{sc_i}(i\omega)\} + \omega^2 \{M_{sc_i}\}) \tag{45}$$

where $[\hat{C}_i(i\omega)]$ is the ith row of $[C(i\omega)]^{-1}$. The measure of importance of the $[Q_{sc}]$ terms is based on Eqs. (44) and (45):

$$[\bar{W}_{cs}]_\ell = q \left| [C(ik_\ell)]^{-1} \left(q\, [Q_{sc}(ik_\ell)] + \frac{k_\ell^2 V^2}{b^2} [M_{sc}] \right) \right|^T / |T_{c_{ii}}(ik_\ell)| \tag{46}$$

The measure of importance of the $[Q_{cc}]$ terms is based on Eq. (44) and its derivative with respect to $Q_{cc_{ii}}$:

$$\bar{W}_{cc_{ij\ell}} = \frac{q}{|T_{c_{ii}}(ik_\ell)|} \tag{47}$$

where the same $\bar{W}$ is assigned to all the terms in the ith row of $[Q_{cc}]$, even though only the diagonal term appears in Eq. (44).

The weighting of $[Q_{cg}]$ is based on the partial derivative of the term that the continuous gust would add to the ith hinge moment of Eq. (44) with respect to $Q_{cg_{ij}}$. The measure of importance is

$$\bar{W}_{cg_{ij\ell}} = \frac{q}{V} \frac{\sqrt{\Phi_{w_j}(k_\ell)}}{|T_{c_{ii}}(ik_\ell)|} \tag{48}$$

The weight matrices assigned to tabulated $[Q_{sc}]$, $[Q_{cc}]$, and $[Q_{cg}]$ matrices are

$$[W_{cs}\ W_{cc}\ W_{cg}]_\ell = \frac{1}{\hat{W}_c} [\bar{W}_{cs_\ell}\ \bar{W}_{cc_\ell}\ \bar{W}_{cg_\ell}] \tag{49}$$

where

$$\hat{W}_c = \max_{i,j,\ell} \{ |Q_{ij}(ik_\ell)| \bar{W}_{ij\ell} \}$$

over all of the hinge-moment-related terms.

Numerical Example

Fighter Aircraft

The first example deals with a fighter aircraft with wing-tip missiles. The purpose of this example is to compare minimum-state results with other methods, to investigate the nonlinear least-square process, and to compare results with different match constraints. The data consist of 12 symmetric vibration modes (2 rigid-body and 10 elastic) and no control or gust modes. The doublet lattice method (DLM) generalized aerodynamic matrices at Mach 0.6 are tabulated at 10 k values of 0, 0.1, 0.3, 0.6, 1.0, 1.3, 1.6, 2.0, 2.3, and 2.5.

Variations of the total approximation error [ϵ_t of Eq. (30)] for five different cases are given in Fig. 1. All of the cases are with the data normalization of Eq. (31). The first two cases are

the extended modified matrix Pade method with variable column roots (EMMP/v) and the ELS method of Roger as outlined in Refs. 10 and 11. Constraints were imposed in both cases to match the data at $k = 0.0$ and at $k_f = k_g = 0.6$, and the approximation roots were optimized for best overall fit using the ISAC computer program. The three other cases of Fig. 1 are of the minimum-state (MS) method. The first MS case is with the same match constraints as the previous methods ($NKF = 4$, where NKF is the index of the nonzero tabulated k value at which both real and imaginary match constraints are imposed). The two other MS cases, both with match constraints at $k = 0.0$ and at $k_f = k_g = 2.5$ ($NKF = 10$), are initiated with different values of $[D]$, as discussed below. The MS approximation roots [the diagonal of $[R]$ of Eq. (18)] are not optimized. The distinct root values were chosen between -0.1 and -5.0. The same roots were used for parallel cases on the three MS curves.

The cases on the MS ($NKF = 4$) curve of Fig. 1 were started with the $m = 5$ case using the default $[D]$ [see definitions following Eq. (29)]. The final $[D]$ of the iterative $D \rightarrow E \rightarrow D$ process for the $m = 5$ case was then expanded with the default columns and used as initial $[D]$ in the $m = 8$ case, and so on from case to case. The initial $[D]$ matrices for the cases on the ($NKF = 10$),1 curve were the final $[D]$ matrices of the parallel case on the ($NKF = 4$) curve. Another approach has been taken for the ($NKF = 10$),2 curve for the sake of consistent investigation of the iterative $D \rightarrow E \rightarrow D$ process. Each case was analyzed independently, starting with the initial default values of $[D]$. The variation of ϵ_t with the number of iterations is given in Fig. 2. The computation time per iteration ranged from 2.5 s for $m = 5$ to 25 s for $m = 20$ on a MicroVax computer.

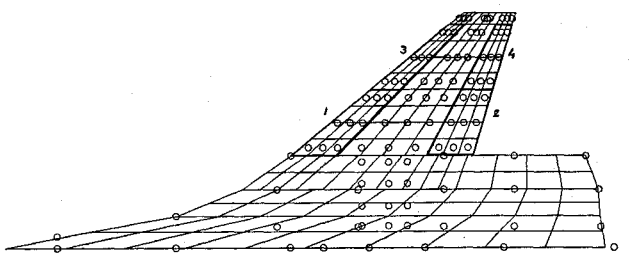

Fig. 3 Top view of the AFW aerodynamic model and structural grids.

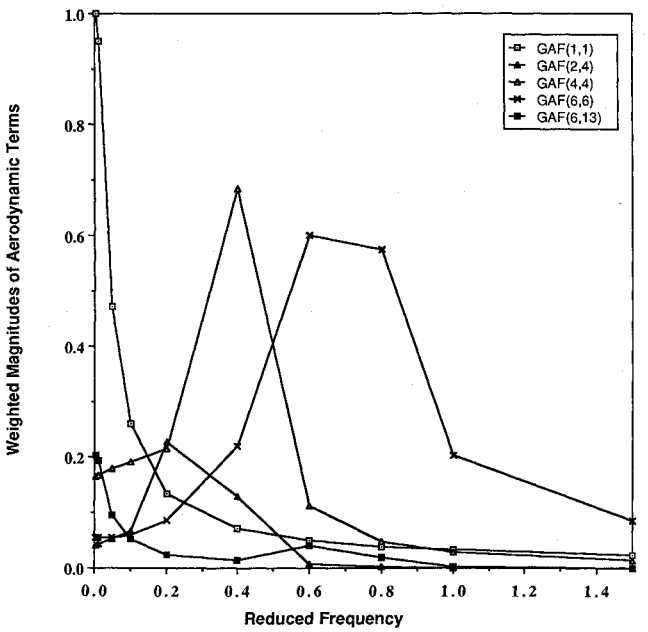

Fig. 4 Weighted magnitudes of aerodynamic terms vs reduced frequency.

It may be concluded from this example that of the various methods, the MS method yields a given accuracy with much fewer augmented states, even without optimization of the approximation roots. It can also be observed for this case that imposing match conditions at the highest k value yields lower total errors. The convergence process and the end results depend on the initial guess of $[D]$, but not very strongly. Numerical divergence, such as that of the $m = 20$ case of Fig. 2, may occur at high m values. This indicates that the amount of data is not sufficient for this high-order approximation, and more k values should be added to the tabulated data. However, it is most likely that the user will find the results to be sufficiently accurate before numerical divergence occurs. Even though no optimization of the minimum-state approximation root values has been performed in this work, the nonunique solution and the nonmonotonic convergence rate of the iterative least-

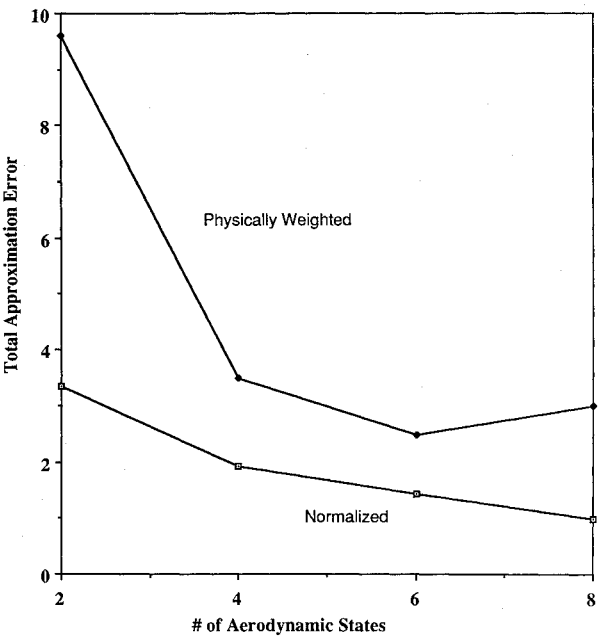

Fig. 5 Minimum-state approximation errors vs number of aerodynamic states.

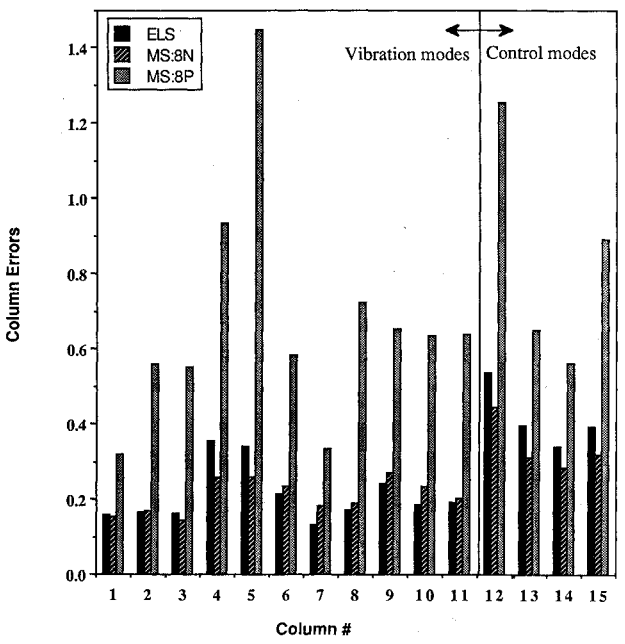

Fig. 6 Column errors in ELS and minimum-state cases.

square process indicate potential difficulties if such optimization is attempted.

AFW Wind-Tunnel Model

This example deals with Rockwell's Active Flexible Wing (AFW) wind-tunnel model to be tested at the Transonic Dynamics Tunnel at the NASA Langley Research Center. A top view of the aerodynamic model is given in Fig. 3. The circles indicate points at which modal data were obtained from the vibration analysis. The mathematical model consists of 15 antisymmetric modes: 1 rigid-body (roll), 10 elastic, and 4 control surface deflection modes. The DLM generalized aerodynamic matrices at Mach 0.9 are tabulated at 12k values of 0, 0.005, 0.01, 0.05, 0.1, 0.2, 0.4, 0.6, 0.8, 1.0, 1.5, and 2.0.

Since gust response is not of interest, and since the actuators are assumed to be irreversible, only $[Q_{ss}]$ and $[Q_{sc}]$ of Eq. (1) are to be approximated. ELS approximation, with three optimized roots (resulting in 33 aerodynamic lag states) and with match constraints at $k=0$ only, have a total approximation error of $\epsilon_t = 1.12$, which is considered satisfactory. A similar error (0.9) is obtained by the MS approximation with $m=8$, match constraints at $k=0$ and at $k_i = k_g = 2.0$, and with the normalization weighting of Eq. (31). The MS approximation has been repeated for eight cases symbolized by mN or mP, where N stands for the normalization weighting, and P stands for the physical weighting of Eqs. (36) and (40). The approximation roots in the MS cases were arbitrarily spaced between the values of -0.1 and -2.4 and were not optimized.

The flow conditions for calculating the physical weights are $V = 5400$ in./s and $q = 1.39$ psi. The control system uses a single roll-rate gyro to activate four third-order actuators of the control surfaces of Fig. 3 through constant gains of 0.0, 0.1, 0.1, and 0.0, respectively. The zero gains are replaced by 0.001 in the weighting process to avoid zero weights to all the elements of the related aerodynamic columns (12 and 15), which would cause singularity in Eq. (26).

The variations of selected weighted magnitudes of aerodynamic terms, $\bar{Q}$ of Eq. (32), with tabulated k values are shown in Fig. 4. These terms belong to the group of only 13.3% of the terms that have a maximum $\bar{Q}$ value of more than 0.1. Diagonal weighted aerodynamic terms have peak values around the natural frequencies of the associated modes. This is also typi-

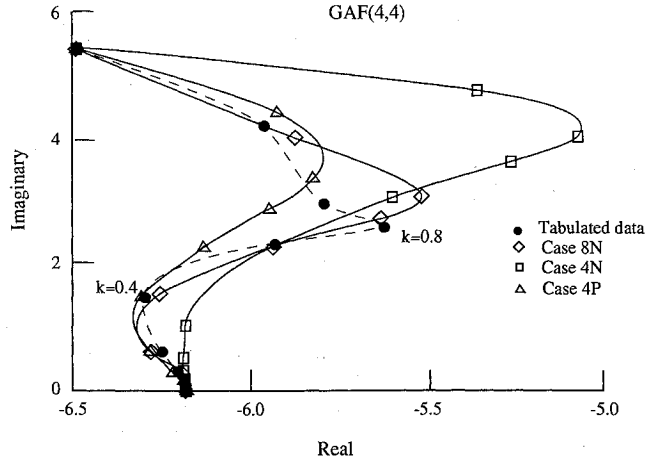

Fig. 7 Minimum-state curve fits for the (4,4) term of the generalized aerodynamic force matrix.

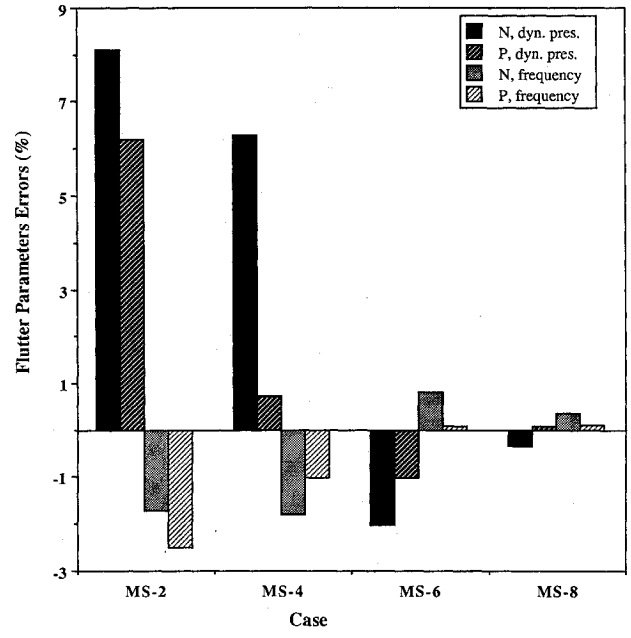

Fig. 8 Flutter dynamic pressure and flutter frequency percentage errors using minimum-state and ELS approximations.

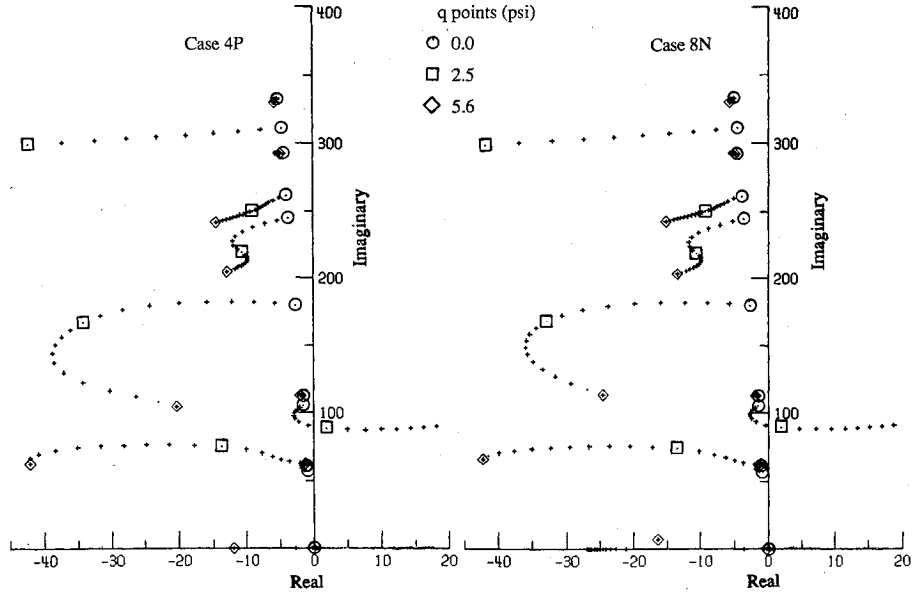

Fig. 9 First-order root-loci vs dynamic pressure for the AFW model.

cal to the diagonal terms associated with modes, 2, 7, 8, and 10 (not shown). The diagonal weights associated with the other modes are several orders of magnitude smaller since these modes are not aeroelastically active, as shown later in this section. The weighted values of terms (6,13) and (2,4) are typical to relatively important control terms and off-diagonal vibration-mode-related terms, respectively. The MS total approximation errors, all calculated by Eq. (30) with the weighting of Eq. (31), are given in Fig. 5. Although the weights of Eq. (31) are those of the normalized cases, they are different than those of the physically weighted cases [defined in Eqs. (36) and (40)]. As a result, a physically weighted case always shows a higher error than that of a normalized cases with the same number of approximation roots.

Column errors of the ELS, $8N$, and $8P$ cases are given in Fig. 6. The total error of the jth column, ϵ_{t_j}, is calculated with Eq. (30), where the $\epsilon^2_{ij\ell}$ terms are summed over the i and ℓ indices only. It can be observed that the control-related terms are relatively harder to fit than others, and that the ELS errors are similar to those of $8N$. The main thing to observe in the $8P$ case is that, even though many weights are several times lower than others, the errors are not excessive.

Approximation curve fits for the (4,4) aerodynamic term are shown in the real-imaginary plane in Fig. 7. This term is relatively hard to fit, but aeroelastically active, as indicated in Fig. 4. It can be observed that the $4P$ minimum-state fit is generally better than the $4N$ fit, especially in the range of relatively high weights ($k=0.2$ to 0.4) where it is as good as the $8N$ case.

The real test of the physical weighting is in the resulting aeroservoelastic characteristics. Second-order closed-loop root-loci calculations have been performed using the STABCAR[18] module of ISAC. In the "baseline" case the program employed the p-k method to calculate p-plane roots with constant velocity and Mach number and variable dynamic pressure, using the same tabulated aerodynamic data as used by the approximated data, and the calculations were repeated for all of the approximation cases. The baseline flutter dynamic pressure is $q_f=2.4$ psi, and the flutter frequency is $\omega_f=89.7$ rad/s ($k=0.33$). The q_f and ω_f percentage errors for the various case are given in Fig. 8. It can be observed that when m is not too small, the physical weighting cuts the flutter errors by a factor of 2 or more. It should be noticed that the flutter dynamic pressure is almost twice that of the nominal q for which the weights were calculated. This indicates that the physical weighting, calculated at one set of flow parameters, has a beneficial effect over a wide parameter range.

Root-loci calculations were also performed with the first-order (state-space) formulation of this paper, expanded to include the actuator dynamics using the DYNARES module of ISAC. The results for the $8N$ and $4P$ cases are plotted in Fig. 9. Differences in the characteristic roots may be observed only for roots that are both far from the imaginary axis and related to dynamic pressures that are more than twice the nominal one.

Conclusions

The minimum-state method for rational approximation of unsteady aerodynamic force coefficients has been modified to allow more combinations of constraints and supplemented with two data-handling algorithms, one for normalization and the other for physical weighting of the tabulated aerodynamic coefficients. The method yields a first-order, linear, aeroservoelastic mathematical model with a relatively low number of aerodynamic augmented states per desired accuracy. Applications to practical aircraft models demonstrate that, with the data normalization, the number of aerodynamic states is about one third of those obtained by other approximation methods with comparable accuracy. Additional significant reduction in model size per desired accuracy of the resulting aeroservoelastic characteristics is obtained when the minimum-state method is combined with the new method of physically weighting the tabulated data.

References

[1]Sevart, F. D., "Development of Active Flutter Suppression Wind Tunnel Testing Technology," Air Force Flight Dynamics Lab., TR-74-124 Jan. 1975.

[2]Edwards, J. W., "Unsteady Aerodynamic Modeling and Active Aeroelastic Control," Stanford Univ., Stanford, CA, SUDAAR 504, Feb. 1977.

[3]Roger, K. L., "Airplane Math Modeling Methods for Active Control Design," AGARD-CP-228, Aug. 1977.

[4]Vepa, R. "Finite State Modeling of Aeroelastic System," NASA CR-2779, Feb. 1977.

[5]Roger, K. L., Hodges, G. E., and Felt, L. "Active Flutter Suppression—A Flight Test Demonstration," *Journal of Aircraft,* Vol. 12, June 1975, pp. 551–556.

[6]Karpel, M. "Design for Active Flutter Suppression and Gust Alleviation Using State-Space Aeroelastic Modeling," *Journal of Aircraft,* Vol. 19, March 1982, pp. 221–227.

[7]Dunn, H. J., "An Analytical Technique for Approximating Unsteady Aerodynamics in the Time Domain," NASA TP-1738, Nov. 1980.

[8]Karpel, M. "Design for Active and Passive Flutter Suppression and Gust Alleviation," NASA CR-3842, Nov. 1981.

[9]Tiffany, S. H. and Adams, W. M., Jr., "Fitting Aerodynamic Forces in the Laplace Domain: An Application of a Nonlinear Nongradient Technique to Multilevel Constrained Optimization," NASA TM-86317, Oct. 1984.

[10]Tiffany, S. H. and Adams, W. M., Jr. "Nonlinear Programming Extensions to Rational Function Approximations of Unsteady Aerodynamics," *Proceedings of the AIAA/ASME/ASCE/AHS 28th Structures, Structural Dynamics, and Materials Conference,* AIAA, New York, 1987, pp. 406–420.

[11]Tiffany, S. H. and Adams, W. M., Jr., "Nonlinear Programming Extension to Rational Approximation Methods of Unsteady Aerodynamic Forces," NASA TP-2776, July 1988.

[12]Bisplinghoff, R. L. and Ashley, H., *Principles of Aeroelasticity,* Wiley, New York, 1962.

[13]Newsom, J. R. "A Method for Obtaining Practical Flutter Suppression Control Laws Using Results of Optimal Control Theory," NASA TP-1671, Aug. 1979.

[14]Arbuckle, P. D., Buttrill, C. S., and Zeiler, T. A., "A New Simulation Model Building Process for Use in Dynamic Systems Integration Research," *Proceedings of the AIAA 1987 Flight Simulation Technologies Conference,* AIAA, New York, 1987, pp. 96–106.

[15]Peele, E. L. and Adams, W. M., Jr., "A Digital Program for Calculating the Interaction Between Flexible Structures, Unsteady Aerodynamics, and Active Controls," NASA TM-80040, Jan. 1979.

[16]Franklin, G. F. and Powell, J. D., "Digital Control of Dynamic Systems," Addison-Wesley, Reading, MA, 1980.

[17]Dryden, H. L., "A Review of the Statistical Theory of Turbulence," *Quarterly of Applied Mechanics,* No. 1, April 1943, pp. 7–42.

[18]Adams, W. M., Jr., Tiffany, S. H., Newsom, J. R., and Peele, E. L., "STABCAR—A Program for Finding Characteristic Roots of Systems Having Transcendental Stability Matrices," NASA TP-2165, June 1984.